ELSEVIER

Journal of Organometallic Chemistry 554 (1998) 63–73

Journal of Organometallic Chemistry

Photochemistry of thin amorphous films of $Fe(CO)_4PPh_3$ on Si(111) surfaces

Sharon L. Blair, Ross H. Hill *

Department of Chemistry, Simon Fraser University, Burnaby, British Columbia, Canada, V5A 1S6

Received 9 January 1997; revised 21 April 1997

Abstract

The photochemical reactions of $Fe(CO)_4PPh_3$ and $Fe(CO)_3(PPh_3)_2$ as amorphous films on silicon surfaces are presented. The mechanism of the reaction of $Fe(CO)_4PPh_3$ in the films has been studied in some detail. Initial CO loss leads to a thermally unstable intermediate, $Fe(CO)_3PPh_3$, which decomposes in the film leading to the production of iron. In thick films photoproduced CO remains trapped in the film and may react with $Fe(CO)_3PPh_3$, regenerating the starting material. Further evidence for this intermediate arises from experiments conducted with PPh_3 added to the film. In these films the initial photoproduct is trapped by PPh_3 yielding $Fe(CO)_3(PPh_3)_2$. A quantitative study of the quantum yield efficiency in these films was undertaken. The $Fe(CO)_3(PPh_3)_2$ films are photosensitive undergoing CO loss to yield $Fe(CO)_2(PPh_3)_2$, as demonstrated by its trapping, by PPh_3, to form $Fe(CO)_2(PPh_3)_3$. Extended photolysis of $Fe(CO)_3(PPh_3)_2$ films, including those containing photoproduced $Fe(CO)_2(PPh_3)_3$, results in the formation of iron. The surface photochemistry of both $Fe(CO)_4PPh_3$, and $Fe(CO)_3(PPh_3)_2$ are shown to be compatible with standard lithography. Patterns of 1×100 μm lines of iron oxide were easily produced on a silicon surface. © 1998 Elsevier Science S.A.

Keywords: Photochemistry; Surface chemistry; Thin films

1. Introduction

Organometallic complexes have been used as precursors to generate thin films of metals and metal oxides by both chemical and photochemical vapor deposition pathways [1–9]. The advantage of the photochemical pathway has been the use of photolysis to direct the deposition process. This is of particular importance in applications where specific coating of a pattern is desirable, such as in the fabrication of microelectronics. Using photolysis to direct the deposition allows for the elimination of a polymer masking step in the fabrication procedure. An additional advantage of the photochemical process is the low process temperature. Our own research has involved the study of inorganic and organometallic complexes in the solid state as precursors to metal and metal oxide films [10–17]. In these studies, films of the precursor complexes are converted photochemically in the solid state to thin films of the metal or its oxide.

Previously we have demonstrated the ability to fabricate metal and metal oxide structures via photolysis of inorganic precursor films through a lithography mask [17,18]. In this process an amorphous film is cast by spin coating. This is followed by the irradiation of the surface film, normally conducted under vacuum, to generate the final metal films. The vacuum appears to be necessary for the production of high quality films as it aids in the diffusion of the photoejected ligands from the surface. In this paper we explore the use of mixtures and quantitative quantum yield information to elucidate the mechanism of the photochemical reactions which occur in the amorphous thin film phase.

The complex studied, $Fe(CO)_4PPh_3$, was chosen for a variety of reasons. The photochemistry of $Fe(CO)_5$ and its substituted derivatives have been examined previously in the gas phase [19], in solution [20], in glasses [21], matrices [22,23] and bound to both polymers [24] and surfaces [25]. This report is, however, the first report of its chemistry in an amorphous thin film.

* Corresponding author.

Precedent suggests that loss of CO, according to Eq. (1), is the dominant primary photoprocess for iron carbonyl complexes.

$$Fe(CO)_4PPh_3 \xrightarrow{h\nu} Fe(CO)_3PPh_3 + CO \quad (1)$$

Reaction in the condensed phase may be expected to result in the formation of a variety of products resultant from the thermal chemistry of this intermediate. Clusters with iron carbonyl phosphines are well-known [26–29].

In this study we have restricted our attention to $Fe(CO)_4PPh_3$. The coordination of a large phosphine, PPh_3, renders the vapor pressure of the complex sufficiently low that evaporation of the starting material during the study is inconsequential. It should be noted that the PPh_3 ligand will have a negative impact on the purity of the photoproduced films. Our concern in this paper is, however, directed at the process investigation rather than the purity of the photoproduced materials.

2. Results

2.1. Spectroscopic data for the complexes

The FTIR spectra of the carbonyl regions of $Fe(CO)_4PPh_3$ and $Fe(CO)_3(PPh_3)_2$ are shown in Fig. 1a and Fig. 2a and are summarized in Table 1. The symmetry of $Fe(CO)_4PPh_3$ is $C_{3\nu}$ and we expect three allowed transitions associated with the CO stretching modes ($2A_1$ and E). All of these bands are observed. For $Fe(CO)_3(PPh_3)_2$ the *trans* isomer is expected to have only one band observed (E in D_{3h} symmetry) while either a $C_{2\nu}$ or a C_s structure would lead to three bands

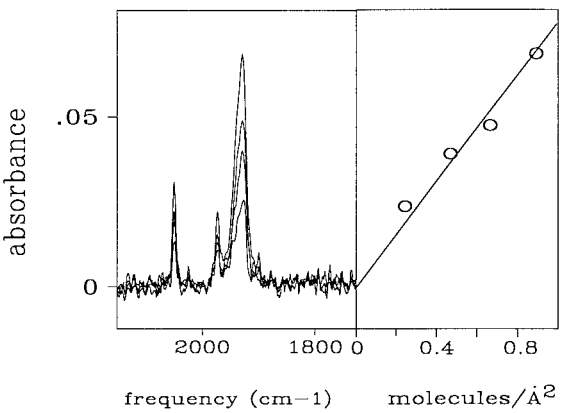

Fig. 1. (a) FTIR spectra associated with 0.21, 0.42, 0.63 and 0.84 molecules of $Fe(CO)_4PPh_3$ per Å^2 on a silicon surface. (b) Plot of absorbance of the 1931 cm^{-1} band of $Fe(CO)_4PPh_3$ versus coverage, data from (a).

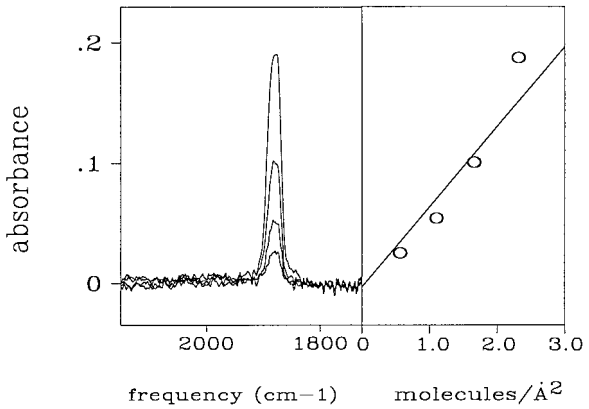

Fig. 2. (a) FTIR spectra associated with 0.56, 1.12, 1.68, 2.24 and 2.80 molecules of $Fe(CO)_3(PPh_3)_2$ per Å^2 on a silicon surface. (b) Plot of absorbance of the ν(CO) band at 1877 cm^{-1} of $Fe(CO)_3(PPh_3)_2$ versus coverage, data from Fig. 1a.

being allowed. From the single observed band we can confirm the *trans* geometry of the phosphine ligands. The absolute frequencies reported here are consistent with the spectra reported in solution [31] and in low-temperature matrices [21]. This similarity in the IR spectra indicates that there are no strong intermolecular interactions in the thin amorphous films. It should be noted that the films studied here are multilayered and that no effect due to the interface with either the silicon surface or the vacuum is spectroscopically observed.

The plots of absorbance versus coverage are shown in Fig. 1b and Fig. 2b. The points on these plots give an approximate estimate of the error associated with the measurement of the absorbance. In practice the absorbance will also depend upon the optical quality of the film deposited. In the case of the evaporative deposition the quality was variable and we believe resulted in the large spread in the data. The data is treated as linear. This observation indicates that the absorbance in the FTIR may be used as an indication of the amount of a species in the film. Throughout this work we will use the absorbance to monitor the extent of reaction in these systems. Similar plots were made for the additive molecules, PPh_3 and $HCPh_3$. Extinction coefficients at selected wavelengths were calculated from these plots and are presented in Table 1.

Electronic absorption spectra for amorphous films of the pure compounds were obtained and the results are summarized in Table 1. Absorption spectra in the films are comparable to results obtained in other media [31]. The extinction coefficients reported in Table 1 were determined by measurements relative to the FTIR bands for which less scattering was expected. In this way we could use optical quality spin-coated films for the determination of these relative extinction coefficients. A direct calibration by electronic absorption spectroscopy

Table 1
FTIR spectral data for relevant complexes on Si(111)

Complex	Assignment	Energy [cm^{-1}] (ε_{IR} [$Å^2$ $molecule^{-1}$])	Absorbance per monolayer	Assignment	Energy [nm] (ε_{UV} [cm^2 mol^{-1}])
$Fe(CO)_4PPh_3$	$\nu_{(CO)}$	2048 (0.031)	0.00047	d–d	366 (3.78×10^6)
	$\nu_{(CO)}$	1973 (0.022)	0.00034	CT	268 (34.4×10^6)
	$\nu_{(CO)}$	1931 (0.073)	0.0011	CT	232 (99.3×10^6)
$Fe(CO_3(PPh_3)_2$	$\nu_{(CO)}$	1877 (0.094)	0.0010	d–d	436 (1.12×10^6)
				d–d	366 (5.77×10^6)
				d–d	348 (7.69×10^6)
				CT	252 (45.0×10^6)
				CT	230 (72.3×10^6)
$Fe(CO)_2(PPh_3)_3^a$	$\nu_{(CO)}$	1894			
	$\nu_{(CO)}$	1838			
PPh_3		1433 (0.0029)	5.8×10^{-5}		
		742 (0.0031)	6.2×10^{-6}		
		694 (0.0044)	8.7×10^{-6}		
$HCPh_3$		1495 (0.0116)	0.00023		

[a] See Ref. [30].

is precluded by problems associated with light scattering at shorter wavelengths for poor quality films.

2.2. Photochemistry of $Fe(CO)_4PPh_3$

The spectroscopic changes resultant from photolysis of thin films of $Fe(CO)_4PPh_3$ are shown in Fig. 3. A decrease in intensity to baseline of all FTIR bands associated with the carbonyl stretching vibrations at 2048, 1973 and 1931 cm^{-1} is observed. This indicates the loss of all starting material. No bands associated with a CO containing photoproduct are apparent. Each band decreases in intensity proportional to its original intensity hence no direct evidence is found for the formation of an intermediate. This is consistent with an initial primary photoprocess yielding a thermally unstable intermediate. This intermediate then undergoes rapid thermal decomposition. This evidence is consistent with Eq. (1) as the initial photochemical step producing thermally unstable $Fe(CO)_3PPh_3$ which undergoes rapid decomposition as shown in Eq. (2).

$$Fe(CO)_3PPh_3 \rightarrow Fe + 3CO + PPh_3 \quad (2)$$

FTIR spectroscopic data following photolysis of the compound indicates loss of all starting material. The resultant films were analyzed by Auger electron spectroscopy to determine if the ejected ligands diffused out of the film. The analysis of films produced from $Fe(CO)_4PPh_3$ are consistent with the loss of CO and PPh_3 from the film leaving a film composed primarily of iron, oxygen, and some residual PPh_3 (Table 2). The surface layer is oxidized, as expected for iron, but depth profiling with argon ions indicates a decreasing oxide content as the film is sputtered. Independent experiments indicate that sputtering causes more efficient loss of carbon than phosphorus from phosphines. This suggests that a significant amount of the carbon found is associated with the phosphine in the film. Further evidence for PPh_3 being retained in the film arises from the depth profiling experiments. In these experiments the surface of the film contains less PPh_3 as indicated by the observation of 1.6% phosphorous. For longer sputtering times the interior of the film is exposed and higher amounts of phosphorus (3.4%) are evident. This result is indicative of efficient loss of PPh_3 from the surface of the film. In the interior of the film, where diffusion is required prior to loss of the PPh_3, more phosphorus is retained.

Previous work [21] in other media indicated that the expected primary photoproduct is $Fe(CO)_3PPh_3$. This coordinatively unsaturated system is known to be sus-

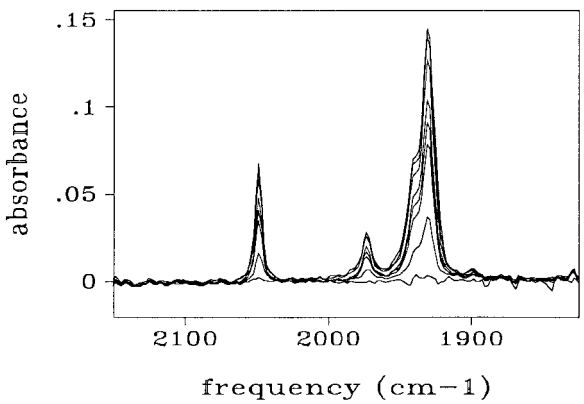

Fig. 3. FTIR spectral changes associated with the photolysis for 0, 60, 120, 210, 270, 330, 600 and 1365 min of a 134-monolayer film of $Fe(CO)_4PPh_3$ deposited on Si(111).

Table 2
Properties of the films: Composition of initial films by FTIR, thickness of the initial films and composition of the final films by Auger analysis

Initial film composition	Initial film thickness (nm)	Sputter time (min)	% Fe	% P	% C	% O
$Fe(CO)_4PPh_3$	273	0	14.1	1.6	68.3	16.1
		3	16.9	3.4	71.8	7.8
$Fe(CO)_3(PPh_3)_2$	34	0.25	10.3	1.9	77.8	7.7
		1	8.6	5.5	77.9	8.0

ceptible to attack by two electron donor ligands, L, to yield $Fe(CO)_3PPh_3L$ [21,32].

In order to investigate if $Fe(CO)_3PPh_3$ was formed in the thin film photoreaction, a film of codeposited $Fe(CO)_4PPh_3$ and PPh_3 was studied. This reaction was done with the aim of trapping the intermediate, $Fe(CO)_3PPh_3$, with PPh_3 to form $Fe(CO)_3(PPh_3)_2$. Spin coating a chip with a solution containing $Fe(CO)_4PPh_3$ and PPh_3 results in the formation of stable amorphous films composed of the compounds. In Fig. 4 the spectroscopic changes resultant from photolysis of a film composed of both PPh_3 and $Fe(CO)_4PPh_3$ are shown.

The loss of carbonyl bands associated with $Fe(CO)_4PPh_3$ is observed and is accompanied by the growth of a new absorption at 1877 cm^{-1}. This band increases in intensity, reaches a maximum and then decays in intensity as a result of further photolysis. The transient band at 1877 cm^{-1} is assigned as due to the production of *trans*-$Fe(CO)_3(PPh_3)_2$. This assignment has been confirmed by comparison with the absorption associated with an authentic sample. This assignment is consistent with the primary photoprocess being loss of the axial CO, forming the $Fe(CO)_3PPh_3$ intermediate as in Eq. (1). This intermediate is trapped by PPh_3 within the film, according to Eq. (3) to form *trans*-$Fe(CO)_3(PPh_3)_2$, in competition with the decomposition reaction of Eq. (2). It is also apparent that a small amount of an additional band due to $Fe(CO)_2(PPh_3)_3$ is observed at 1838 cm^{-1} (the other band due to this species at 1894 cm^{-1} is obscured). The formation of $Fe(CO)_2(PPh_3)_3$ is associated with the subsequent photoreactions of *trans*-$Fe(CO)_3(PPh_3)_2$ and is treated separately below.

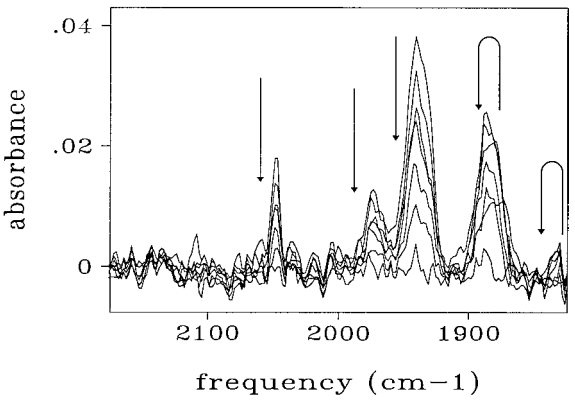

Fig. 4. FTIR spectral changes associated with the photolysis for 0, 5, 10, 15, 20, 30, and 75 min of a 27-monolayer film of $Fe(CO)_4PPh_3$ codeposited with PPh_3 deposited on Si(111). Note several additional spectra were recorded for this experiment.

$$Fe(CO)_3PPh_3 + PPh_3 \rightarrow Fe(CO)_3(PPh_3)_2 \quad (3)$$

In order to assess the efficiency of the trapping reaction of Eq. (3) in competition with the decomposition of Eq. (2), studies were done in which the amount of PPh_3 within the film was varied. The efficiency of trapping can be expressed as the ratio of *trans*-$Fe(CO)_3(PPh_3)_2$ formed to $Fe(CO)_4PPh_3$ lost. The results of several experiments indicated that when no PPh_3 is added to the film no *trans*-$Fe(CO)_3(PPh_3)_2$ is observed. The exception to this occurs when thick films are monitored at long photolysis times. In these instances the photoproduced PPh_3 is sufficient to produce detectable amounts of *trans*-$Fe(CO)_3(PPh_3)_2$. For films with PPh_3 added the initial ratio of *trans*-$Fe(CO)_3(PPh_3)_2$ formed to $Fe(CO)_4PPh_3$ lost is within error of 1 regardless of the concentration of PPh_3 within the film; as long as some *trans*-$Fe(CO)_3(PPh_3)_2$ is observed. Due to the photosensitivity of *trans*-$Fe(CO)_3(PPh_3)_2$ this ratio decreases as the photolysis continues. The photoreaction of the *trans*-$Fe(CO)_3(PPh_3)_2$ ultimately results in a low steady state concentration of *trans*-$Fe(CO)_3(PPh_3)_2$.

2.3. Quantum yield studies on $Fe(CO)_4PPh_3$

The variation in quantum yields with reaction conditions were studied. The effect of both film thickness and additives on the quantum yield for disappearance of $Fe(CO)_4PPh_3$ was studied. First the effect of film thickness on the quantum yield will be presented.

For a relatively thick film of $Fe(CO)_4PPh_3$, irradiation led to loss of absorption bands associated with the starting material and no intermediate was evident, Fig. 3. A plot of absorbance versus irradiation time was fit to an exponential decay as shown in Fig. 5. The decay constant can be converted to quantum efficiency and was found to be $(3.8 \pm 0.5) \times 10^{-4}$.

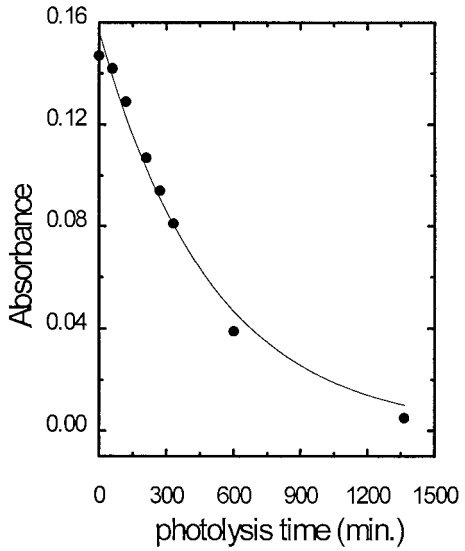

Fig. 5. Plot of absorbance at 1931 cm^{-1} versus photolysis time for a 134-monolayer film of $Fe(CO)_4PPh_3$, the data was derived from Fig. 3.

The dependence of the photoefficiency of $Fe(CO)_4PPh_3$ on film thickness was studied in some detail. Films of varying thickness were prepared and the photochemistry monitored for each film. The quantum yields are reported in Table 3. The general trend is that as the film thickness increases the quantum yield decreases. A detailed interpretation of this result is presented in Section 3. Before considering the interpretation of these quantum yields the influence of additives on the quantum yield will be presented.

The effect of air on the reaction efficiency was investigated. When films were monitored in an air atmosphere, the spectral changes were similar to those observed in a vacuum. The quantum efficiency of the reaction in air was much higher than for films of comparable thickness under vacuum. The data in Table 3 indicates an order of magnitude increase in the quantum yield as a result of conducting the photochemistry under an air atmosphere.

The quantum yield for reaction of the films containing both $Fe(CO)_4PPh_3$ and PPh_3 can be determined from spectral changes upon photolysis. Control experiments indicate that films containing both $Fe(CO)_4PPh_3$ and PPh_3 are thermally sensitive. This complication allows only a qualitative assessment of the effect of additives on the quantum yield for decomposition. The spectral changes presented in Fig. 4 for a film containing 27 monolayers $Fe(CO)_4PPh_3$ and 48 monolayers PPh_3 were used to determine the quantum yield. The quantum yield for the loss of $Fe(CO)_4PPh_3$ in films composed in part of PPh_3 can be calculated from an exponential fit of A_t versus irradiation time as shown in Fig. 6. The decay constant, in conjunction with light intensity and extinction coefficient yields the quantum yield as 0.047 ± 0.02. This value is significantly larger than the quantum yield in the absence of the PPh_3 additive. The combination of both air and PPh_3 results in a similar increase in the quantum yield as shown in Table 3.

When an inert substance such as $HCPh_3$ is added to the film the photoproduct is unchanged and the quantum yield is not significantly altered as indicated in Table 3. Before considering the detailed interpretation of these results the photochemistry of $Fe(CO)_3(PPh_3)_2$ will be presented in Section 2.4.

2.4. Photochemistry of $Fe(CO)_3(PPh_3)_2$

The observation of photoproduced *trans*-$Fe(CO)_3(PPh_3)_2$ resultant from the photolysis of a film composed of both PPh_3 and $Fe(CO)_4PPh_3$ was confirmed by comparison of the FTIR spectrum obtained with that due to an authentic sample. Prolonged photol-

Table 3
Quantum yields for decomposition of $Fe(CO)_4PPh_3$ in thin films

Coverage [molecule/Å^{-2}] (monolayers)	A_o	Quantum yield (error)[a]	Additives	Coverage[b] [molecules Å^{-2}] (monolayers)	Atmosphere
0.10 (7)	0.0076	0.0032 (0.001)			Vacuum
0.50 (33)	0.0362	0.0016 (0.0002)			Vacuum
0.66 (44)	0.0484	0.0023 (0.0008)			Vacuum
1.18 (78)	0.0862	0.0007 (0.0001)			Vacuum
2.01 (134)	0.147	0.00038 (0.00005)			Vacuum
0.97 (64)	0.0707	0.0043 (0.004)			Air
1.12 (74)	0.0817	0.011 (0.002)			Air
0.4 (27)	0.0293	0.047 (0.02)[c]	PPh_3	9.8 (48)	Vacuum
1.35 (89)	0.0984	0.048 (0.01)[c]	PPh_3	7.9 (39)	Air
1.18 (79)	0.0865	0.0009 (0.0001)	$HCPh_3$	0.395 (20)	Vacuum

[a] Error calculated from exponential decay fit.
[b] calculated from absorbance.
[c] Error high due to competing thermal reaction.

ysis of the film composed of both PPh_3 and $Fe(CO)_4PPh_3$ led to loss of all peaks including those associated with the *trans*-$Fe(CO)_3(PPh_3)_2$ photoproduct. It was therefore necessary to establish that samples of *trans*-$Fe(CO)_3(PPh_3)_2$ were photochemically active. Films of this complex exhibit a single ν(CO) at 1877 cm^{-1}. Photolysis of a thin film of *trans*-$Fe(CO)_3(PPh_3)_2$ results in the decrease in intensity of the single CO band as illustrated in Fig. 7. No new absorption bands associated with a possible intermediate species are observed. The overall reaction initiated by photolysis occurs as in Eq. (4). Further evidence for the loss of all ligands from the complex comes from the Auger analysis which is consistent with the loss of all ligands yielding a somewhat impure (Table 2) iron surface.

$$Fe(CO)_3(PPh_3)_2 \xrightarrow{h\nu} Fe + 3CO + 2PPh_3 \quad (4)$$

One interpretation is that photolysis of *trans*-$Fe(CO)_3(PPh_3)_2$ results in CO loss leading to the thermally unstable species $Fe(CO)_2(PPh_3)_2$. This would be consistent with the absence of any observable iron carbonyl photoproduct. The thermal decomposition of $Fe(CO)_2(PPh_3)_2$ would lead to iron, carbon monoxide and PPh_3. An alternative reactivity would be the loss of the PPh_3 ligand from *trans*-$Fe(CO)_3(PPh_3)_2$ leading to the unstable $Fe(CO)_3PPh_3$ discussed above. These two scenarios would be expected to be affected differently by the addition of PPh_3 to the film. In the first mechanism, involving CO loss, the presence of uncoordinated PPh_3 in the film would be expected to result in the trapping of $Fe(CO)_2(PPh_3)_2$ and the production of $Fe(CO)_2(PPh_3)_3$. The presence of PPh_3 would not be expected to alter the products of the phosphine loss mechanism. However, trapping of $Fe(CO)_3PPh_3$ in this mechanism would regenerate *trans*-$Fe(CO)_3(PPh_3)_2$ resulting in a decrease in the observed quantum yield for decomposition.

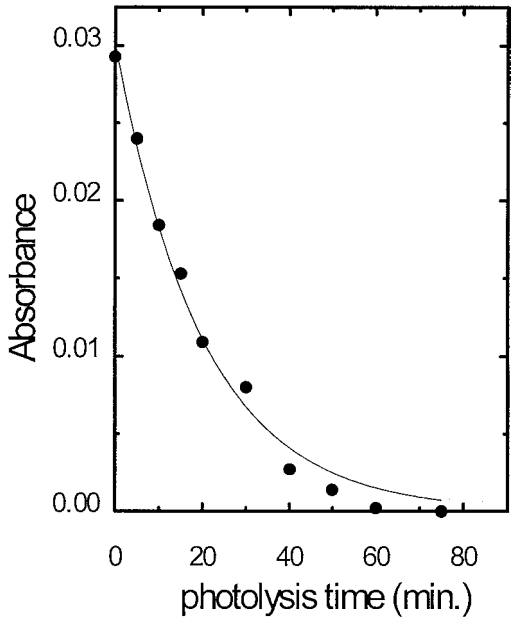

Fig. 6. Plot of the absorbance at 1931 cm^{-1} versus photolysis time for a 27-monolayer film of $Fe(CO)_4PPh_3$ codeposited with PPh_3. The data is derived from the experiment of Fig. 4, although data left out of Fig. 4 is included.

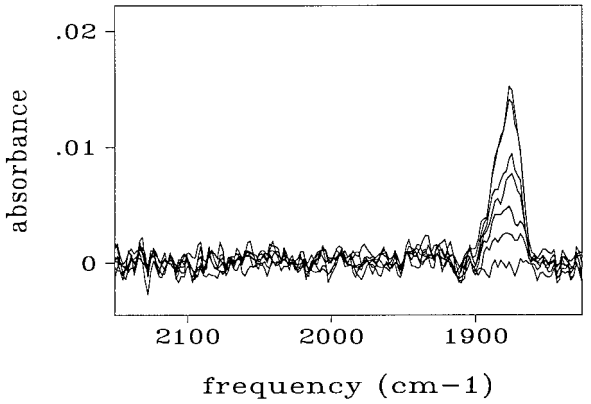

Fig. 7. FTIR spectral changes associated with the photolysis for 0, 2, 15, 30, 60, 120 and 245 min of a 17-monolayer film of $Fe(CO)_3(PPh_3)_2$.

In order to investigate the primary photoreaction of *trans*-$Fe(CO)_3(PPh_3)_2$ thin films with PPh_3 codeposited were prepared and studied. Photolysis of these films would be expected to yield $Fe(CO)_2(PPh_3)_3$ if the initial photoreaction was CO loss. Irradiation results in the loss of intensity at 1877 cm^{-1} associated with the single absorption band of *trans*-$Fe(CO)_3(PPh_3)_2$. Concomitant growth of a band at 1838 cm^{-1} is observed. This band is attributed to the formation of $Fe(CO)_2(PPh_3)_3$. The second band associated with $Fe(CO)_2(PPh_3)_3$, expected at 1894 cm^{-1} [30], is obscured by the band at 1877 cm^{-1} associated with the starting material. The steady-state concentration of this species was quite small. The production of $Fe(CO)_2(PPh_3)_3$ is also apparent from Fig. 4. In this figure the continued photolysis of the film composed of both PPh_3 and $Fe(CO)_4PPh_3$ led to the production of *trans*-$Fe(CO)_3(PPh_3)_2$. The photolysis of this photoproduct led to the formation of $Fe(CO)_2(PPh_3)_3$ as evidenced by the production of a band at 1838 cm^{-1}.

The observation of $Fe(CO)_2(PPh_3)_3$ production from photolysis of $Fe(CO)_3(PPh_3)_2$ confirms that at least one reaction pathway of $Fe(CO)_3(PPh_3)_2$ must be CO loss. For this reason we favor the interpretation that photolysis of $Fe(CO)_3(PPh_3)_2$ results in the loss of CO yielding $Fe(CO)_2(PPh_3)_2$ according to Eq. (5). The coordinatively unsaturated intermediate may either decompose (Eq. (6)) or, in the presence of PPh_3, react to form $Fe(CO)_2(PPh_3)_3$ (Eq. (7)). The $Fe(CO)_2(PPh_3)_3$ photo-

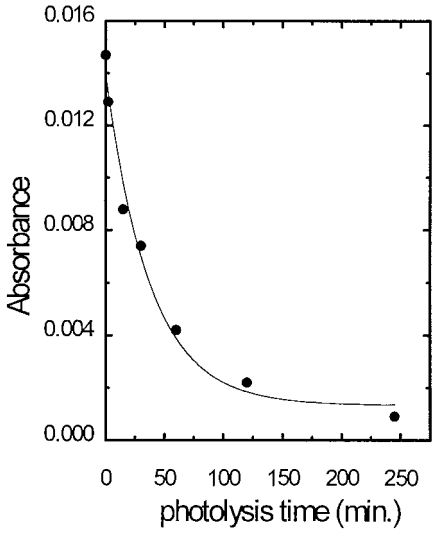

Fig. 8. Plot of the absorbance at 1877 cm^{-1} versus photolysis time for a 14-monolayer film of $Fe(CO)_3(PPh_3)_2$, the data is derived from the experiment of Fig. 7.

product is known to have a labile PPh_3 ligand [33]. If it lost a PPh_3 it would likely decompose.

$$Fe(CO)_3(PPh_3)_2 \xrightarrow{h\nu} Fe(CO)_2(PPh_3)_2 + CO \quad (5)$$

$$Fe(CO)_2(PPh_3)_2 \rightarrow Fe + 2CO + 2PPh_3 \quad (6)$$

$$Fe(CO)_2(PPh_3)_2 + PPh_3 \rightarrow Fe(CO)_2(PPh_3)_3 \quad (7)$$

The alternative dissociative photoreaction of $Fe(CO)_3(PPh_3)_2$ is shown in Eq. (8). This would not give rise to independently detectable products and so we cannot rule out this pathway. However, if Eq. (8) adequately describes the photochemistry of this system then we expect that the photoefficiency of the reaction of $Fe(CO)_3(PPh_3)_2$ in films containing PPh_3 should be lower than of those containing no PPh_3. This is expected to result from trapping the photogenerated $Fe(CO)_3PPh_3$ intermediate. Alternatively if the sequence of reactions shown in Eqs. (5)–(7) is dominant, then the addition of PPh_3 would be expected to result in an increase in the quantum yield for decomposition of

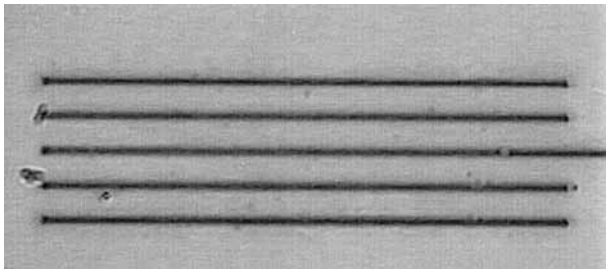

Fig. 9. Optical micrograph of surface obtained by the photolithography of $Fe(CO)_4PPh_3$ on a silicon(111) surface. An internal scale is provided by the 50-μm length of the lines.

$Fe(CO)_3(PPh_3)_2$. This would result from the trapping according to Eq. (7) which would prevent any thermal reversal of Eq. (5). Quantum yields for the photodecomposition of $Fe(CO)_3(PPh_3)_2$ in films both with and without PPh_3 were measured in order to further investigate these possibilities.

$$Fe(CO)_3(PPh_3)_2 \xrightarrow{h\nu} Fe(CO)_3(PPh_3) + PPh_3 \quad (8)$$

2.5. Quantum yield studies on $Fe(CO)_3(PPh_3)_2$

The quantum yields for the photoreaction of $Fe(CO)_3(PPh_3)_2$ were also determined by monitoring the decay of starting material as a function of photolysis time. In Fig. 8 the decay of the 1877 cm^{-1} absorbance band of $Fe(CO)_3(PPh_3)_2$ is plotted against photolysis time and fit to an exponential decay. The resultant quantum yield is 0.004 ± 0.001. Similar experiments were conducted on samples with additives and thicker films. The results are summarized in Table 4.

The results indicate that a large increase in the quantum yield is associated with the addition of PPh_3 to the film. In this system we find no quantum yield variation associated with the film thickness. Table 4 shows that films which range in thickness from 13 to 75 nm have the same quantum yield. This result supports the contention that Eqs. (5)–(7) represent the major reaction pathway.

Table 4
Quantum yields for reaction of $Fe(CO)_3(PPh_3)_2$ in thin films

Coverage [molecules $Å^{-2}$] (monolayers)	A_o	Quantum yield[a]	Additives	Coverage[b] [molecules $Å^{-2}$] (monolayers)	Atmosphere
0.16 (15)	0.0147	0.004 (0.001)			Vacuum
0.84 (79)	0.0788	0.006 (0.001)			Vacuum
0.36 (34)	0.0337	0.07 (0.04[c])	PPh_3	3.0(14)	Vacuum
0.28 (26)	0.0262	0.012 (0.007[c])	PPh_3	4.3(21)	Air

[a] Error calculated from fit.
[b] Calculated from absorbance.
[c] Error high due to competing thermal reaction.

2.6. Lithography

This surface photochemistry is compatible with lithography allowing us to pattern surfaces. This was demonstrated by irradiation of a surface film of $Fe(CO)_4PPh_3$ through a lithography mask. The mask was set up in contact with the surface negating the need for optics. The result of this procedure is shown in Fig. 9. Clear formation of lines 1 μm by 50 μm are visible.

3. Discussion

The photolysis of thin amorphous films of $Fe(CO)_4PPh_3$ on silicon wafers results in the decomposition of this species with no observed intermediates. This result is somewhat surprising in view of the known photochemistry of iron carbonyl under a variety of conditions. For example, low-temperature matrix studies indicate that the formation of products associated with the loss of a single ligand are readily trapped at low temperature [23]. While this result in not directly transferable to the film environments, related studies in polymers indicate that such intermediates are stable under conditions where no diffusion motion is allowed and there are no opportunities for reaction. In this case, one may speculate that the formation of iron–iron bonds may provide the mechanism for decomposition although it is not clear why no bands associated with dimers or clusters are observed.

The evidence presented here supports a mechanism summarized in Scheme 1. Initial photolysis of $Fe(CO)_4PPh_3$ results in CO loss. The product, $Fe(CO)_3PPh_3$, is not sufficiently stable to be observed spectroscopically under our conditions. This species may decompose to iron, releasing all ligands, back react with the photogenerated CO or, in the presence of PPh_3, generate $Fe(CO)_3(PPh_3)_2$. Photolysis of $Fe(CO)_3(PPh_3)_2$ leads to a similar set of reactions. Photoejection of CO to form $Fe(CO)_2(PPh_3)_2$ may be followed by decomposition, reaction with photogenerated CO to reform the starting material, or trapping by PPh_3 to yield $Fe(CO)_2(PPh_3)_3$. Finally, the photolysis of $Fe(CO)_2(PPh_3)_3$ results in CO loss to produce $Fe(CO)(PPh_3)_3$. This photoproduct is unstable and may either decompose or react with photogenerated CO. While this interpretation of the reaction mechanism is relatively straightforward consideration of the efficiency of the reaction yields further intricate details.

The quantum yield for this process has been measured for a variety of film thickness and is presented in Table 3. Thin films have a higher quantum yield for decomposition. The simplest interpretation of this data is related to the reaction of uncoordinated CO with the unsaturated intermediate, $Fe(CO)_3PPh_3$. The intermediate was demonstrated above to be sufficiently stable to react with PPh_3 yielding $Fe(CO)_3(PPh_3)_2$. It is hence reasonable to expect that the photoproduced $Fe(CO)_3PPh_3$ within the film may be able to also trap the photogenerated CO according to Eq. (9). Thicker films would hence be expected to retain more CO leading to more efficient trapping and an overall lower quantum yield. The quantum yield for decomposition, Φ^D, may be expressed as a function of the quantum yield for loss of CO, Φ^0, times the fraction which thermally decomposes prior to trapping by CO as shown in Eq. (10).

$$Fe(CO)_3PPh_3 + CO \rightarrow Fe(CO)_4 + PPh_3 \quad (9)$$

$$\Phi^D = \Phi^0 \frac{k_2}{k_1[CO] + k_2} \quad (10)$$

A plot of $(\Phi^D)^{-1}$ versus [CO] is expected to yield a straight line. In our case the source of CO is the

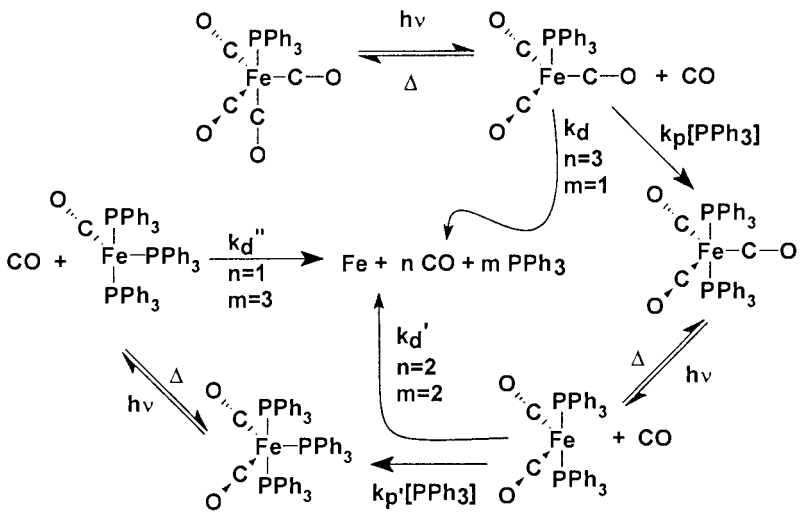

Scheme 1. Proposed reaction sequence for photolysis of $Fe(CO)_4PPh_3$ in multilayer films.

reaction itself. For thick films the quantum yield decreases with time, indicating a buildup of CO in the film. For thin films this does not occur indicating that CO diffuses out of the film and does not attain a sufficient concentration to alter the quantum yield. No direct measure of [CO] within the film is available although an estimate for the dependence of film thickness may be made.

Assuming the rate of diffusion of CO within a film is constant then the CO concentration will be a function of the thickness of the film. In the simplest case we can think of the effusion of the gas from the film being affected by the thickness. Under these conditions we assume the proportion of CO retained, and hence [CO] to be related directly to film thickness. Under these qualitative assumptions we have Eq. (11) where L is the thickness in monolayers of the film and c is the proportionality constant.

$$\frac{1}{\Phi^{D}} = \frac{k_1 cL}{\Phi^{0} k_2} + \frac{1}{\Phi^{0}} \qquad (11)$$

If the steady-state concentration of CO within the film is proportional to the film thickness then a plot of $(\Phi^{D})^{-1}$ versus film thickness is expected to be linear. This plot is presented in Fig. 10 and the linearity is surprising. The slope of this line, 22 ± 2 nm^{-1}, has no obvious significance since we have no way to relate the thickness to the absolute concentration of CO. It is important to note that the intercept, 69.46 ± 124, is within the expected range. For an initial quantum yield of 1 we expect an intercept of 1 (well within our error). The found intercept indicates a quantum yield for CO loss of 0.014 although a large error is associated with this. The lower limit for this yield is 0.005. The data does not establish an upper limit for the quantum yield.

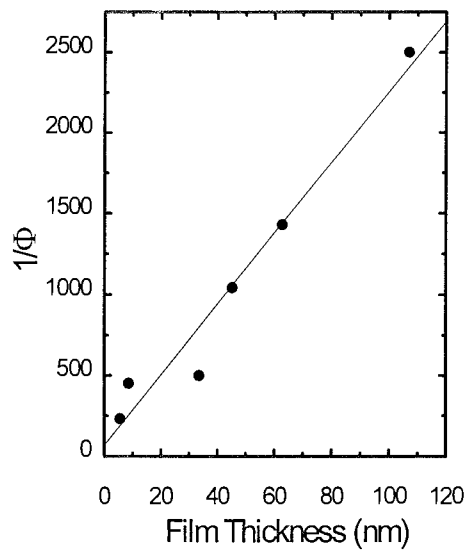

Fig. 10. Plot of the reciprocal of the quantum yield for decomposition of $Fe(CO)_4PPh_3$, in thin films versus film thickness.

The reaction of PPh_3 with the unsaturated intermediate should lead to an increase in the quantum yield. The quantum yield variation resultant from a change in film composition is presented in Table 3. This data clearly indicates that the introduction of PPh_3 in the film results in an increase in the quantum yield. Unfortunately the increase in thermal reactivity precludes a quantitative study of the quantum yield. This system is more complex to model because a change in the composition will affect not only the physical properties of the film but also the chemistry. The qualitative result does, however, indicate an increase in quantum yield associated with the addition of PPh_3.

These results are consistent with the set of reactions shown within Scheme 1. Photoinduced loss of the axial CO results in the formation of $Fe(CO)_3PPh_3$. This species is thermally unstable and undergoes rapid decomposition yielding iron films. Some recoordination of CO occurs in thick films. In the presence of a coordinating ligand, such as PPh_3, the intermediate is stabilized by the coordination of the added ligand. In the case of PPh_3, the product of association is $Fe(CO)_3(PPh_3)_2$.

Two key pieces of evidence must be considered at this juncture. First, the qualitative trend established that the quantum yield increased with increasing PPh_3 content in the film. However, the addition of PPh_3 resulted in a 100% trapping efficiency of the initial photoproduct, $Fe(CO)_3PPh_3$, generating $Fe(CO)_3(PPh_3)_2$. The trapping efficiency did not increase with increasing PPh_3 content in the film. The observation of this behavior with codeposited $HCPh_3$ is particularly informative. This additive is not expected to coordinate and lead to no evident trapping of an intermediate. The addition of $HCPh_3$ did not result in an increase in the quantum yield for the reaction. This latter fact allows us to rule out an effect due to the concentration of the starting material within the film. In view of these two factors we can also draw some conclusions regarding the trapping of $Fe(CO)_3PPh_3$ by PPh_3.

At low concentrations of PPh_3 in the film the $Fe(CO)_3PPh_3$ is effectively trapped in competition with decomposition. This trapping results in an effective chemical yield of 100% for *trans*-$Fe(CO)_3(PPh_3)_2$ formation. When the amount of PPh_3 in the film is increased the quantum yield increases with no change in the chemical yield. This is consistent with the PPh_3 effectively competing with the CO recombination reaction. This competition results in the increase in the overall quantum yield for reaction.

4. Conclusions

Photochemical studies of amorphous films of $Fe(CO)_4PPh_3$ showed a dependence of quantum yield on film thickness. The primary photoreaction, loss of

CO, is irreversible in thin films resulting in loss of all ligands. In thick films, the ejected CO does not diffuse through the film as efficiently and, as a result reacts with the $Fe(CO)_3PPh_3$ intermediate. This combination results in the observation of lower quantum yields for thicker films. When the initial film is a mixture of $Fe(CO)_4PPh_3$ and PPh_3 the intermediate reacts with PPh_3 forming $Fe(CO)_3(PPh_3)_2$ which is photosensitive. Independent photochemical studies of pure $Fe(CO)_3(PPh_3)_2$ resulted in loss of all ligands with no observable intermediate. This system was demonstrated to be compatible with current lithography techniques. However, Auger analysis indicated that the resultant films were contaminated with phosphorus. This was expected, due to the low volatility of PPh_3. For practical applications the incorporation of a more volatile ligand, such as in $Fe(CO)_4PEt_3$ would be preferable.

5. Experimental

The silicon wafers were obtained from Pacific Microelectronics Center, Canada. The Si(111) surface was used in these studies and the wafers were p-type silicon with tolerances and specifications as per SEMI Standard M1.1.STD.5 cut to the approximate dimensions of 1 cm $\times$ 1.5 cm in house. The CaF_2 crystals were obtained from Wilmad Glass.

The FTIR spectra were obtained with 4 cm^{-1} resolution using a Bomem Michelson 120 FTIR spectrophotometer. The samples were held in an anodized aluminum sample mount within a NaCl faced vacuum chamber. Electronic absorption spectra were obtained with a HP 8452A diode array spectrometer.

The photolysis beam was a 100 W high-pressure Hg lamp in an Oriel housing equipped with condenser lenses and filtered through a 10 cm water filter with quartz optics. Additional filters (band pass 350–400 nm) to isolate the 366 emission line were used.

Auger spectra were obtained using a PHI double pass CMA at 0.85 eV resolution at the Surface Physics Laboratory, Department of Physics, Simon Fraser University. Film thickness was determined using a Leitz Laborlux 12 ME S optical microscope with an interference attachment.

The chromium plated quartz lithography mask was kindly donated by IBM.

The complexes, $Fe(CO)_4PPh_3$, $Fe(CO)_3(PPh_3)_2$, were prepared by literature procedures [31,34].

5.1. Calibration of absorption on the surface

A stock solution of $Fe(CO)_4PPh_3$ (0.0134 g) was prepared in CH_2Cl_2 (5 ml). This solution was then diluted by a factor of 10 with CH_2Cl_2. A drop (0.0045 ml) of this solution was then deposited on the surface of a silicon wafer. The solvent was allowed to evaporate and the FTIR spectrum obtained. This process was repeated several times yielding the spectra shown in Fig. 1a. The area over which the film was deposited was measured to be 0.79 cm^2. Each drop of the solution corresponds to a coverage of 0.21 molecules per $Å^2$. The corresponding calibration curve of absorbance versus molecules per $Å^2$ for the absorbance at 1931 cm^{-1} is shown in Fig. 1b. The slope of this line yields an absorbance of 0.073 ($\pm$10%) $Å^2$ $molecule^{-1}$. Assuming a molecular volume of approximately (8.1 Å)^3, this corresponds to an absorbance of approximately 0.0011 per monolayer for the absorption at 1931 cm^{-1}. The corresponding extinction coefficients of the other bands were obtained from their relative intensity and are presented in Table 1.

The same treatment of a solution prepared from $Fe(CO)_3(PPh_3)_2$ (0.0055 g) in methylene chloride (5.0 ml) resulted in each drop contributing 0.56 molecules $Å^{-2}$ to the film. The spectra for sequential drops are illustrated in Fig. 1a and the resultant calibration curve is shown in Fig. 2b. An absorbance of 0.094 ($\pm$14%) $Å^2$ $molecule^{-1}$ is found for the single absorbance at 1877 cm^{-1}. The molecular volume of this molecule is approximately (9.5 Å)^3 and the absorbance is 0.0010 per monolayer.

The electronic absorption spectra were obtained by spin-coating samples onto CaF_2 plates and calibrated by comparison with FTIR obtained on these samples. The energies of the electronic transitions are obtained directly while the extinction coefficients were obtained relative to the calibrated intensities of the infrared transitions. Energies and extinction coefficients for both compounds are reported in Table 1.

5.2. Photolysis of complexes as films on silicon surfaces

All photolysis experiments were done in the same manner. For example, a Si(111) surface was prepared with $Fe(CO)_4PPh_3$ by dispensing a single drop of a CH_2Cl_2 solution containing the iron complex onto a spinning silicon chip. This resulted in the formation of a uniform, amorphous coating of the chip. The chip was then transferred to a vacuum Dewar. The system was placed under vacuum and the FTIR spectrum obtained. The sample was then irradiated for 60 min and another FTIR spectrum was obtained. This procedure was repeated for the following (accumulated) photolysis times: 120, 210, 270, 330, 600 and 1365 min. The spectra are presented in Fig. 3.

The intensity of the light source was measured with an International Light IL1350 Radiometer and the photon output at 366 nm was 9.45×10^{-9} E s^{-1} cm^{-2}. The output of the light source was found to be constant (within error 10%) by periodic measurement of intensity throughout the experiments.

The quantum yields were calculated as described previously [12,17]. In cases where curvature was evident in the plots only the first 10% was used to calculate the quantum yield.

The sample was then moved to the Scanning Auger Microprobe for elemental analysis of the surface. The results are presented in Table 2.

In some experiments PPh_3 was codeposited with $Fe(CO)_4PPh_3$ from a single solution containing both components. The result of photolysis of this sample is shown in Fig. 4. Spectral results for the photolysis of $Fe(CO)_3(PPh_3)_2$ are illustrated in Fig. 8.

5.3. Lithography

A film containing $Fe(CO)_4PPh_3$ was spin-coated onto a silicon(111) surface, as described in Section 5.2. The thickness of the film was measured by optical interferometry and found to be 137 nm. The sample was placed in contact with a lithography mask and irradiated through a 10 cm water filter and the mask using a 150 W Xe high pressure lamp for 36 h. The sample was removed and rinsed with methylene chloride to dissolve the unexposed starting material. The image presented in Fig. 7 was obtained with a Leitz Laborlux ME 2 S optical microscope.

Acknowledgements

We wish to thank B. Heinrich and K. Myrtle of the Surface Physics Laboratory, Simon Fraser University, for assistance in obtaining the Auger spectra. We thank NSERC (Canada) for financial support.

References

[1] M.J. Almond, D.A. Rice, C.A. Yates, Chem. Br. 24 (1988) 1130.
[2] M.J. Rand, J. Electrochem. Soc. 120 (1973) 686.
[3] R. Kumar, M. Rashidi, R.J. Puddephatt, Polyhedron 8 (1989) 551.
[4] N.H. Dryden, R. Kumar, E. Ou, M. Rashidi, S. Roy, P.R. Norton, R.J. Puddephatt, Chem. Mater. 3 (1991) 677.
[5] H.H. Gilgen, T. Cacouris, P.S. Shaw, R.R. Krchnavek, R.M. Osgood, Appl. Phys. B 42 (1987) 55.
[6] D.K. Liu, R.J. Chin, A.L. Lai, Chem. Mater. 3 (1991) 13.
[7] J.S. Foord, R.B. Jackman, Chem. Phys. Lett. 112 (1984) 190.
[8] V. Borker, K.S. Rane, V.N. Kamat Dalal, J. Mater. Sci. 4 (1993) 241.
[9] G. Frolov, V.S. Zhigalov, S.M. Zharkov, I.R. Yarullin, Phys. Solid State 36 (1994) 526.
[10] B.J. Palmer, A. Becalska, R.H. Hill, J. Photochem. Photobiol. A: Chem. 57 (1991) 457.
[11] B.J. Palmer, A. Becalska, R. Hader, R.H. Hill, Polyhedron 10 (1991) 877.
[12] A. Becalska, R.J. Batchelor, F.W.B. Einstein, R.H. Hill, B.J. Palmer, Inorg. Chem. 31 (1992) 3118.
[13] D.G. Bickley, R.H. Hill, C.I. Horvath, J. Photochem. Photobiol. A: Chem. 67 (1992) 181.
[14] T.W.H. Ho, S.L. Blair, R.H. Hill, D.G. Bickley, J. Photochem. Photobiol. A: Chem. 69 (1992) 229.
[15] B.J. Palmer, R.H. Hill, J. Photochem. Photobiol. A: Chem. 72 (1993) 243.
[16] S.L. Blair, W. Xia, R.H. Hill, J. Photochem. Photobiol. A: Chem. 81 (1994) 183.
[17] B.J. Palmer, A. Becalska, T.W.H. Ho, R.H. Hill, J. Mater. Sci. 28 (1993) 6013.
[18] S.L. Blair, J. Hutchins, R.H. Hill, D.G. Bickley, J. Mater. Sci. 29 (1994) 2143.
[19] J.T. Yardley, B. Gitlin, G. Nathanson, A.M. Rosan, J. Chem. Phys. 74 (1981) 370.
[20] G.L. Geoffroy, M.S. Wrighton, Organometallic Photochemistry, Academic Press, New York, 1979.
[21] D.K. Liu, C. Brinkley, M.S. Wrighton, Organometallics 3 (1984) 1449.
[22] M. Poliakoff, J.J. Turner, J. Chem. Soc., Faraday Trans. 70 (1974) 93.
[23] M. Poliakoff, J. Chem. Soc., Dalton Trans. (1974) 210.
[24] R.D. Sanner, R.G. Austin, M.S. Wrighton, W.D. Honnick, C.U. Pittman, Inorg. Chem. 18 (1979) 928.
[25] D. Sunil, J. Sokolov, M.H. Rafailovich, X. Duan, H.D. Gafney, Inorg. Chem. 32 (1993) 4489.
[26] A. Shojaie, J.D. Atwood, Organometallics 4 (1985) 187.
[27] S.B. Butts, D.F. Shriver, J. Organomet. Chem. 169 (1979) 191.
[28] P.A. Dawson, B.M. Peake, B.H. Robinson, J. Simpson, Inorg. Chem. 19 (1980) 465.
[29] S.M. Grant, A.R. Manning, Inorg. Chim. Acta 31 (1978) 41.
[30] T.R. Gaffney, J.A. Ibers, Inorg. Chem. 21 (1982) 2851.
[31] H.L. Conder, M.Y. Darensburg, J. Organomet. Chem. 67 (1974) 93.
[32] S.K. Nayak, T.J. Burkey, J. Am. Chem. Soc. 115 (1993) 6391.
[33] H.C. Achton, A.R. Manning, Inorg. Chim. Acta 71 (1983) 163.
[34] F.A. Cotton, R.V. Parish, J. Chem. Soc. (1960) 1440.